

***Ab initio* theory of superconductivity. II. Application to elemental metals**M. A. L. Marques,^{1,2} M. Lüders,^{2,3} N. N. Lathiotakis,^{1,2} G. Profeta,⁴ A. Floris,^{1,5} L. Fast,^{2,6} A. Continenza,⁴ E. K. U. Gross,^{1,2} and S. Massidda^{5,*}¹*Institut für Theoretische Physik, Freie Universität Berlin, Arnimallee 14, D-14195 Berlin, Germany*²*Institut für Theoretische Physik, Universität Würzburg, Am Hubland, D-97074 Würzburg, Germany*³*Daresbury Laboratory, Warrington WA4 4AD, United Kingdom*⁴*CASTI—Istituto Nazionale Fisica della Materia (INFN) and Dipartimento di Fisica, Università degli studi dell'Aquila, I-67010 Coppito (L'Aquila) Italy*⁵*INFN SLACS, Sardinian Laboratory for Computational Materials Science and Dipartimento di Scienze Fisiche, Università degli Studi di Cagliari, S. P. Monserrato-Sestu km 0.700, I-09124 Monserrato (Cagliari), Italy*⁶*SP Swedish National Testing and Research Institute, P. O. Box 857, S-501 15 Borås, Sweden*

(Received 1 June 2004; revised manuscript received 25 February 2005; published 29 July 2005)

The density functional theory for superconductors developed in the preceding article is applied to the calculation of superconducting properties of several elemental metals. In particular, we present results for the transition temperature, for the gap at zero temperature, and for thermodynamic properties like the specific heat. We obtain an unprecedented agreement with experimental results. Superconductors with both strong and weak electron-phonon coupling are equally well described. This demonstrates that, as far as conventional superconductivity is concerned, the first-principles prediction of superconducting properties is feasible.

DOI: [10.1103/PhysRevB.72.024546](https://doi.org/10.1103/PhysRevB.72.024546)

PACS number(s): 74.25.Jb, 74.25.Kc, 74.20.-z, 74.70.Ad

I. INTRODUCTION

The recent discovery of superconductivity¹ at around 40 K in MgB₂ has renewed the attention of the scientific community on this field. MgB₂ is just one in a long list of materials that are found to be superconducting. This list includes several elemental metals, heavy-fermion compounds, high- T_c ceramics,² fullerenes doped with alkali-metal atoms,³ etc. The mechanism responsible for superconductivity can have different origins. For example, in the elemental metals, in the fullerenes,³ and also in MgB₂,^{4,5} the electron-phonon interaction is responsible for the binding of the Cooper pairs. This situation is usually referred to as “conventional superconductivity.” On the other hand, it is generally believed that the very high transition temperatures exhibited by the high- T_c compounds are (at least partly) due to Coulombic effects. Following the remarkable experimental discoveries of the last years, there were numerous theoretical developments that have greatly improved our description and understanding of superconductivity. However, the prediction of material-specific properties of superconductors still remains one of the great challenges of modern condensed-matter theory.

In this work, we present an *ab initio* theory to describe the superconducting state. It is based on a density functional formulation, and is capable of describing both weakly and strongly coupled superconductors. This is achieved by treating the electron-phonon and Coulomb interactions on the same footing. The main equation of this theory resembles the gap equation of the theory of Bardeen, Cooper, and Schrieffer.⁶ It is, however, free of any adjustable parameter and contains effects originating from the retarded nature of the electron-phonon interaction. The theoretical foundations of our approach are presented in the preceding paper,⁷ which will henceforth be referred to as I. As in ordinary density functional theory (DFT),^{8–10} the complexities of the many-

body problem are included in an exchange-correlation functional. In I we use Kohn-Sham perturbation theory¹¹ to derive several approximations for this quantity. In the present paper we describe the implementation of our theory, and its application to the calculation of superconducting properties of elemental metals. The systems under consideration range from weak-coupling (Mo,Al,Ta) to strong-coupling (Nb,Pb) superconductors. By studying these well-known systems, we illustrate the usefulness and accuracy of DFT for superconductors. Furthermore, our results serve as a justification for the choices and approximations made in I. Further applications of our approach to more complex systems like MgB₂ (Ref. 5) or solids under pressure will be presented in separate publications.

This paper is organized as follows. In Sec. II we give a brief summary of the theoretical foundations of our work. The exchange-correlation functionals are described in Sec. III. We present three different levels of approximation: functionals that retain the full dependence on the wave vector, energy-averaged functionals, and hybrid schemes. We proceed with an account of the computational details of our numerical implementation. In Sec. V we present and discuss numerical results obtained for the elemental metals. These results include calculations of the transition temperature T_c , the gap at zero temperature Δ_0 , and thermodynamic properties like the specific heat. The last section is devoted to the conclusions.

II. METHOD

In this section we give a brief account of the theoretical foundations of DFT for the superconducting state. For an in depth description of this theory, we refer the reader to I.

A correct description of the superconducting state has to include the effects of the electron-electron and electron-

phonon interactions. DFT for superconductors is a theory designed to treat on the same footing both electronic correlations and the electron-phonon coupling. To achieve this unified description, we start with the full electron-nuclear Hamiltonian. A multicomponent DFT (Ref. 12) is then established using a set of three densities: (i) the normal electronic density $n(\mathbf{r})$; (ii) the anomalous density $\chi(\mathbf{r}, \mathbf{r}')$, which is the order parameter of the superconducting state; and (iii) the diagonal of the nuclear density matrix $\Gamma(\mathbf{R})$, where \mathbf{R} is a shorthand for the N nuclear coordinates $\{\mathbf{R}_1, \mathbf{R}_2, \dots, \mathbf{R}_N\}$. An extension of the Hohenberg-Kohn theorem^{8,13} guarantees a one-to-one correspondence between the set of the densities $\{n(\mathbf{r}), \chi(\mathbf{r}, \mathbf{r}'), \Gamma(\mathbf{R})\}$ in thermal equilibrium and the set of their conjugate potentials. As a consequence, all observables are functionals of this set of densities.

We then construct a Kohn-Sham system⁹ composed of noninteracting (but superconducting) electrons and nuclei. The latter interact with each other through an N -body potential, but do not interact with the electrons. The Kohn-Sham system is chosen such that the Kohn-Sham densities are equal to the densities of the interacting system. The Euler-Lagrange equations for the Kohn-Sham system lead to a set of three coupled equations, one describing the nuclear degrees of freedom, and the other two describing the electrons. These three equations have to be solved self-consistently. The nuclear equation describes a set of N nuclei under the influence of an effective N -body potential $v_s^n[n, \chi, \Gamma](\mathbf{R})$, and has the same structure as the usual Born-Oppenheimer equation for the nuclei. In this paper we are interested in solids at relatively low temperature, where the nuclei perform small oscillations around their equilibrium positions. In this case, we can expand $v_s^n[n, \chi, \Gamma](\mathbf{R})$ in a Taylor series around the equilibrium positions, and transform the nuclear degrees of freedom into collective (phonon) coordinates. The Kohn-Sham electrons obey a system of two coupled equations

$$\left[-\frac{\nabla^2}{2} + v_s^e(\mathbf{r}) - \mu \right] u_{nk}(\mathbf{r}) + \int d^3r' \Delta_s(\mathbf{r}, \mathbf{r}') v_{nk}(\mathbf{r}') = E_{nk} u_{nk}(\mathbf{r}), \quad (1a)$$

$$-\left[-\frac{\nabla^2}{2} + v_s^e(\mathbf{r}) - \mu \right] v_{nk}(\mathbf{r}) + \int d^3r' \Delta_s^*(\mathbf{r}, \mathbf{r}') u_{nk}(\mathbf{r}') = E_{nk} v_{nk}(\mathbf{r}). \quad (1b)$$

Note that for a periodic solid, we can classify the corresponding solutions according to the symmetry of the translational group of the crystal. Thus we label the eigenstates with a principal quantum number n and a wave-vector quantum number \mathbf{k} . Equations (1) have the same structure as the Bogoliubov–de Gennes equations, and describe a system of non-interacting, superconducting electrons moving under the influence of the effective potential $v_s^e(\mathbf{r})$ and the effective pairing field $\Delta_s(\mathbf{r}, \mathbf{r}')$. As is usual in DFT, the effective potentials $\{v_s^e, \Delta_s, v_s^n\}$ are functionals of the set of densities $\{n, \chi, \Gamma\}$ and include Hartree and exchange-correlation contributions. These latter terms, the exchange-correlation potentials, are defined as functional derivatives with respect to

the densities of the exchange-correlation contribution to the free energy F_{xc} .

The full self-consistent solution of the three Kohn-Sham equations is a highly demanding task. For the time being, we resort to some additional approximations in order to simplify the problem. First, we neglect the dependence of the nuclear potential v_s^n on χ , which amounts to neglecting the effect of the superconducting pair potential on the phonon dispersion. This effect has been measured experimentally,¹⁴ and it turns out to be quite small. Furthermore, we assume that the nuclear potential v_s^n is well approximated by the Born-Oppenheimer potential. Within these approximations, the phonon frequencies and the electron-phonon coupling constants can be calculated using standard density functional linear-response methods.¹⁵

A direct solution of the Kohn-Sham Bogoliubov–de Gennes equations¹⁶ (1) is faced with the problem that one needs extremely high accuracy to resolve the superconducting energy scale, which is about three orders of magnitude smaller than typical electronic energies. At the same time, one has to cover the whole energy range of the electronic band structure. The problem can be simplified through the decoupling approximation.¹⁷ First we assume that $v_s^e(\mathbf{r})$ does not depend significantly on the anomalous density χ . In fact, we expect that corrections to $v_s^e(\mathbf{r})$ are of the order of $|\chi|^2$ and therefore much smaller than the typical electronic energy scale. The normal-state Kohn-Sham eigenfunctions and eigenenergies can then be used to construct approximations for the eigenstates of the superconducting phase

$$u_{nk}(\mathbf{r}) \approx u_{nk} \varphi_{nk}(\mathbf{r}), \quad v_{nk}(\mathbf{r}) \approx v_{nk} \varphi_{nk}(\mathbf{r}). \quad (2)$$

The φ_{nk} 's are the solutions of the normal-state Kohn-Sham equations for band n and wave vector \mathbf{k} and can thus be calculated using standard electronic-structure methods. If N_b is the number of bands, the decoupling approximation transforms, for every \mathbf{k} point in the Brillouin zone, the $2N_b \times 2N_b$ eigenvalue problem given by Eq. (1) into $N_b(2 \times 2)$ secular equations. The Kohn-Sham eigenenergies then become

$$E_{nk} = \sqrt{\xi_{nk}^2 + |\Delta_{nk}|^2}, \quad (3)$$

where ξ_{nk} are the normal-state Kohn-Sham eigenvalues measured relative to the chemical potential $\xi_{nk} = \epsilon_{nk} - \mu$. The matrix elements Δ_{nk} , which are a central quantity in our formalism, are defined as

$$\Delta_{nk} = \int d^3r \int d^3r' \varphi_{nk}^*(\mathbf{r}) \Delta_s(\mathbf{r}, \mathbf{r}') \varphi_{nk}(\mathbf{r}'). \quad (4)$$

Within the decoupling approximation, Δ_{nk} is determined by the integral equation

$$\Delta_{nk} = -\mathcal{Z}_{nk} \Delta_{nk} - \frac{1}{2} \sum_{n'k'} \mathcal{K}_{nk, n'k'} \frac{\tanh[(\beta/2)E_{n'k'}]}{E_{n'k'}} \Delta_{n'k'}, \quad (5)$$

where β is the inverse temperature. The quantities \mathcal{Z}_{nk} and $\mathcal{K}_{nk, n'k'}$ are functionals of the pair potential Δ_{nk} and of the chemical potential μ . We note that, although the gap equa-

tion (5) is static (i.e., it does not depend explicitly on the frequency), it includes retardation effects through the functionals \mathcal{Z}_{nk} and $\mathcal{K}_{nk,n'k'}$. We will come back to this point later in the discussion of our results.

It is possible to view the decoupling approximation from a different perspective: It can be shown that the matrix elements of the pair potential $\Delta_s(\mathbf{r}, \mathbf{r}')$ are diagonal with respect to all symmetry-related quantum numbers, in particular the Bloch wave vector \mathbf{k} , but also labels of the point-group symmetry (which usually are not explicitly given). The decoupling approximation amounts to neglecting the matrix elements which are off diagonal with respect to the band index n . For a given \mathbf{k} point in the Brillouin zone, the corresponding states are in general energetically far apart, which justifies the neglect of these matrix elements. The only situation where this approximation may break down is when two bands of the same symmetry cross in the vicinity of the Fermi surface. We note in passing that the decoupling approximation is (trivially) exact for the uniform superconducting electron gas.

The decoupling approximation can further be justified by the fact that a perturbative treatment of the neglected off-diagonal terms does not give any contribution in first order.¹⁸ To see this, we consider the neglected part of the pair potential

$$\tilde{\Delta}(\mathbf{r}, \mathbf{r}') = \sum_{k,n \neq n'} \varphi_{nk}(\mathbf{r}) \tilde{\Delta}_{k,nn'} \varphi_{n'k'}^*(\mathbf{r}') \quad (6)$$

and treat it by perturbation theory. The first-order correction to the eigenenergies E_{nk} is given by

$$\delta E_{nk}^{(1)} = \int d^3r \int d^3r' u_{nk}^*(\mathbf{r}) \tilde{\Delta}(\mathbf{r}, \mathbf{r}') v_{nk}(\mathbf{r}') + \text{H.c.} \quad (7)$$

Inserting the eigenfunctions $u_{nk}(\mathbf{r})$ and $v_{nk}(\mathbf{r})$ within the decoupling approximation, as given by Eq. (2), and using the orthogonality of the Bloch wave functions, $\int d^3r \varphi_{nk}^*(\mathbf{r}) \varphi_{n'k'}(\mathbf{r}) = \delta_{nn'}$, one finds

$$\delta E_{nk}^{(1)} = u_{nk}^* v_{nk} \sum_{n_1 \neq n_2} \tilde{\Delta}_{k,n_1 n_2}(\mathbf{r}') \delta_{nn_1} \delta_{n_2 n} + \text{H.c.} = 0. \quad (8)$$

Equation (3) allows us to interpret $2\Delta_{nk}$ as the superconducting gap. As a matter of principle, there is no guarantee that this gap reproduces the true gap of the superconductor: Even with the exact exchange-correlation (xc) functional, the Kohn-Sham system need not reproduce the true spectrum of the fully interacting system. In semiconductors and insulators, the fundamental gap is given by the Kohn-Sham gap plus the discontinuity of the xc potential with respect to the particle number. Standard functionals such as the local density approximation and the generalized gradient approximation are continuous with respect to the particle number and, therefore, cannot reproduce the discontinuity. In the superconducting case, the appearance of a discontinuity is not expected because we are not working with fixed particle number in the first place. This fact alone, of course, does not prove that, for superconductors, the Kohn-Sham gap result-

ing from the exact xc functional would be identical with the true gap. This question remains the subject of future investigations.

III. FUNCTIONALS

A. k -dependent functionals

In this work we use the partially linearized versions for the functionals \mathcal{Z}_{nk} and $\mathcal{K}_{nk,n'k'}$ proposed in I. The contributions stemming from the electron-phonon interaction are obtained with the help of Kohn-Sham perturbation theory. There are two terms. (i) The first is nondiagonal

$$\mathcal{K}_{nk,n'k'}^{\text{ph}} = \frac{2}{\tanh[(\beta/2)\xi_{nk}]\tanh[(\beta/2)\xi_{n'k'}]} \sum_{\lambda,q} |g_{\lambda,q}^{nk,n'k'}|^2 \times [I(\xi_{nk}, \xi_{n'k'}, \Omega_{\lambda,q}) - I(\xi_{nk}, -\xi_{n'k'}, \Omega_{\lambda,q})], \quad (9)$$

where $g_{\lambda,q}^{nk,n'k'}$ are the electron-phonon coupling constants and the function I is defined as

$$I(\xi, \xi', \Omega) = f_{\beta}(\xi) f_{\beta}(\xi') n_{\beta}(\Omega) \left[\frac{e^{\beta\xi} - e^{\beta(\xi'+\Omega)}}{\xi - \xi' - \Omega} - \frac{e^{\beta\xi'} - e^{\beta(\xi+\Omega)}}{\xi - \xi' + \Omega} \right]. \quad (10)$$

In the previous expression f_{β} and n_{β} are the Fermi-Dirac and Bose-Einstein distributions. (ii) The second contribution is diagonal in nk and reads

$$\mathcal{Z}_{nk}^{\text{ph}} = \frac{1}{\tanh[(\beta/2)\xi_{nk}]} \sum_{n'k'} \sum_{\lambda,q} |g_{\lambda,q}^{nk,n'k'}|^2 [J(\xi_{nk}, \xi_{n'k'}, \Omega_{\lambda,q}) + J(\xi_{nk}, -\xi_{n'k'}, \Omega_{\lambda,q})], \quad (11)$$

where the function J is defined by

$$J(\xi, \xi', \Omega) = \tilde{J}(\xi, \xi', \Omega) - \tilde{J}(\xi, \xi', -\Omega). \quad (12)$$

Finally we have

$$\tilde{J}(\xi, \xi', \Omega) = -\frac{f_{\beta}(\xi) + n_{\beta}(\Omega)}{\xi - \xi' - \Omega} \left[\frac{f_{\beta}(\xi') - f_{\beta}(\xi - \Omega)}{\xi - \xi' - \Omega} - \beta f_{\beta}(\xi - \Omega) f_{\beta}(-\xi' + \Omega) \right]. \quad (13)$$

On the other hand, the Coulomb interaction leads to the term

$$\mathcal{K}_{nk,n'k'}^{\text{TF-ME}} = v_{nk,n'k'}^{\text{TF}} \quad (14)$$

with the definition

$$v_{nk,n'k'}^{\text{TF}} = \int d^3r \int d^3r' v^{\text{TF}}(\mathbf{r} - \mathbf{r}') \times \varphi_{nk}^*(\mathbf{r}) \varphi_{nk}(\mathbf{r}') \varphi_{n'k'}(\mathbf{r}) \varphi_{n'k'}^*(\mathbf{r}'). \quad (15)$$

The electronic contribution is written in terms of the matrix elements (MEs) of the screened Coulomb potential, as the use of the bare potential would be unrealistic. In this work we use a very simple model for the screening, namely, the Thomas-Fermi (TF) model

$$v^{\text{TF}}(\mathbf{r}-\mathbf{r}') = \frac{e^{-k_{\text{TF}}|\mathbf{r}-\mathbf{r}'|}}{|\mathbf{r}-\mathbf{r}'|}, \quad (16)$$

with the Thomas-Fermi screening length k_{TF} given by

$$k_{\text{TF}}^2 = 4\pi N(0). \quad (17)$$

Finally, $N(0)$ denotes the total density of states at the Fermi level. Within this approach, the MEs are calculated using the Bloch functions of the real material. In this basis, the MEs read (using standard notation)

$$v_{nk,n'k'}^{\text{TF}} = \frac{1}{\mathcal{V}} \sum_{\mathbf{G}} \frac{4\pi}{|\mathbf{k}-\mathbf{k}'+\mathbf{G}|^2 + k_{\text{TF}}^2} \left| \langle n'k' | e^{-i(\mathbf{k}-\mathbf{k}'+\mathbf{G})\cdot\mathbf{r}} | nk \rangle \right|^2, \quad (18)$$

where \mathcal{V} is the volume of the unit cell.

B. Energy-averaged functionals

As discussed in the previous section, to obtain the gap function Δ_{nk} , we solve the gap equation (5) with the functionals given by Eqs. (9) and (11) for the electron-phonon interaction, and by Eq. (15) for the Coulomb repulsion. The inputs required for such calculation are the electron-phonon coupling constants $g_{\lambda,q}^{nk,n'k'}$, and the normal-state Kohn-Sham eigenenergies ξ_{nk} and eigenfunctions φ_{nk} . The coupling constants can be obtained from linear response¹⁵ DFT calculations, while the eigenstates are the basic output of any standard DFT code.

It is possible, however, to further simplify the solution of Eq. (5). Very often, in the context of Eliashberg theory,¹⁹ one neglects the gap anisotropy over the Fermi surface. We can apply the same approximation in our context (see Ref. 20 for further details). We assume that the pair potential is constant on isoenergy surfaces, i.e., it depends on the energies only:

$$\Delta_{nk} = \Delta(\xi_{nk}). \quad (19)$$

We then insert the unity $1 = \int d\xi \delta(\xi - \xi_{n'k'})$ under the $n'k'$ summation in the right-hand side of Eq. (5), multiply the whole equation with the factor $\delta(\xi - \xi_{nk})$, and perform the summation over all nk . Finally we divide the resulting equation by the density of states at the energy ξ , $N(\xi) = \sum_{nk} \delta(\xi - \xi_{nk})$. This yields the gap equation in energy space, which now is only a one-dimensional integral equation:

$$\begin{aligned} \Delta(\xi) = & -\mathcal{Z}(\xi)\Delta(\xi) \\ & - \frac{1}{2} \int_{-\mu}^{\infty} d\xi' N(\xi') \mathcal{K}(\xi, \xi') \frac{\tanh[(\beta/2)E']}{E'} \Delta(\xi'). \end{aligned} \quad (20)$$

The energy-averaged functions $\mathcal{K}(\xi, \xi')$ and $\mathcal{Z}(\xi)$ are defined as

$$\mathcal{K}(\xi, \xi') = \frac{1}{N(\xi)N(\xi')} \sum_{nk,n'k'} \delta(\xi - \xi_{nk}) \delta(\xi' - \xi_{n'k'}) K_{nk,n'k'}, \quad (21)$$

$$\mathcal{Z}(\xi) = \frac{1}{N(\xi)} \sum_{nk} \delta(\xi - \xi_{nk}) Z_{nk}. \quad (22)$$

We should mention that in performing the average over isoenergetic surfaces we assumed an s -wave pairing field. It is straightforward to devise similar averaging procedures for pairing fields of different symmetry.

The phononic contributions to the averaged functionals read

$$\begin{aligned} \mathcal{K}^{\text{ph}}(\xi, \xi') = & \frac{2}{\tanh[(\beta/2)\xi] \tanh[(\beta/2)\xi']} \frac{1}{N(0)} \int d\Omega \alpha^2 F(\Omega) \\ & \times [I(\xi, \xi', \Omega) - I(\xi, -\xi', \Omega)] \end{aligned} \quad (23)$$

and

$$\begin{aligned} \mathcal{Z}^{\text{ph}}(\xi) = & \frac{1}{\tanh[(\beta/2)\xi]} \int_{-\mu}^{\infty} d\xi' \int d\Omega \alpha^2 F(\Omega) \\ & \times [J(\xi, \xi', \Omega) + J(\xi, -\xi', \Omega)], \end{aligned} \quad (24)$$

with I and J given by Eqs. (10) and (12). Finally, the Eliashberg spectral function is the electron-phonon coupling constant averaged on the Fermi surface,

$$\begin{aligned} \alpha^2 F(\Omega) = & \frac{1}{N(0)} \sum_{nk,n'k'} \sum_{\lambda,q} |g_{\lambda,q}^{nk,n'k'}|^2 \\ & \times \delta(\xi_{nk}) \delta(\xi_{n'k'}) \delta(\Omega - \Omega_{\lambda,q}). \end{aligned} \quad (25)$$

Note that in Eq. (25) [and, consequently, in Eq. (23)] we replaced the density of states $N(\xi)$ by its value at the Fermi energy $N(0)$. This procedure is well justified, because it only requires that for each given band the couplings do not change much on an energy scale of the order of the Debye frequency, i.e., meV. The energy dependence of the density of states, on the other hand, is kept in Eqs. (20) and (22), as $N(\xi)$ can vary even on this small energy scale (e.g., in transition metals where the Fermi energy is at the edge of large peaks in the density of states).

In order to evaluate the Coulomb terms, we further approximate the Kohn-Sham eigenvalues by a free-electron (FE) parabolic dispersion $\varepsilon_k = k^2/2$. This approximation is well justified for simple metals, but it is expected to fail for more complicated systems. Within this approximation the energy average of the Thomas-Fermi screened Coulomb interaction, given in Eq. (18), reads

$$\mathcal{K}^{\text{TF-FE}}(\xi, \xi') = \frac{\pi}{kk'} \ln \left[\frac{(k+k')^2 + k_{\text{TF}}^2}{(k-k')^2 + k_{\text{TF}}^2} \right] \quad (26)$$

with $k = \sqrt{2(\xi - \mu)}$ and $k' = \sqrt{2(\xi' - \mu)}$.

C. Hybrid functionals

It is possible to obtain a hybrid approach where the averaged functionals are used in the \mathbf{k} -dependent gap equation (5). The averaged phononic terms (23) and (24) can be used in Eq. (5), just by replacing the energies ξ and ξ' by the energy eigenvalues of the real material ξ_{nk} and $\xi_{n'k'}$:

$$\mathcal{K}_{nk,n'k'}^{\text{ph}} = \mathcal{K}^{\text{ph}}(\xi_{nk}, \xi_{n'k'}), \quad (27)$$

TABLE I. Summary of the different methods used in our calculations.

Method	Gap equation	Phononic terms	Coulomb term
TF-ME	k dependent Eq. (5)	Hybrid: averaged with real bands Eqs. (23) and (24)	Matrix elements Eq. (18)
TF-SK	k dependent Eq. (5)	Hybrid: averaged with real bands Eqs. (23) and (24)	Hybrid: averaged with real bands Eq. (29)
TF-FE	Energy averaged Eq. (20)	Averaged Eqs. (23) and (24)	Averaged Eq. (26)

$$\mathcal{Z}_{nk}^{\text{ph}} = \mathcal{Z}^{\text{ph}}(\xi_{nk}). \quad (28)$$

For the electronic terms we use an approach that goes along the lines of Sham and Kohn (SK),²¹ as detailed in I. The basic idea is again to replace the free-electron bands by the real bands of the material, and furthermore to adjust the chemical potentials of the two systems. The functional reads

$$\mathcal{K}_{nk,n'k'}^{\text{TF-SK}} = \frac{\pi}{2\sqrt{\eta_{nk}\eta_{n'k'}}} \times \ln\left(\frac{\eta_{nk} + \eta_{n'k'} + 2\sqrt{\eta_{nk}\eta_{n'k'} + k_{\text{TF}}^2/2}}{\eta_{nk} + \eta_{n'k'} - 2\sqrt{\eta_{nk}\eta_{n'k'} + k_{\text{TF}}^2/2}}\right). \quad (29)$$

In this expression we defined $\eta_{nk} = \xi_{nk} + \frac{1}{2}k_{\text{F}}^2$, where k_{F} is the Fermi wave vector of a homogeneous electron gas with (constant) density equal to the average density of the material.

IV. COMPUTATIONAL DETAILS

Obtaining superconducting properties through the solution of the gap equation can be viewed as postprocessing results of standard electronic structure calculations. In this work we used electronic band structures obtained from full-potential linearized augmented plane-wave²² calculations; the same method is also used to compute the Coulomb potential matrix elements (18), along the lines described in Ref. 23. On the other hand, the Eliashberg function can be obtained from linear response calculations.¹⁵ (Note that the Eliashberg functions can also be extracted from experiment. While the use of such experimental α^2F 's renders the theory semiphenomenological it often gives useful insights.)

We developed two completely independent codes: the first solves the averaged gap equation (20) in energy space; the second solves the k -resolved gap equation (5). The two schemes were compared whenever possible, and give similar results for the simple metals studied here (see the discussion at the end of this section). The solution of the averaged gap equation is a quite simple numerical task. The energy is discretized in a logarithmic mesh in order to increase the accuracy close to the Fermi level and the resulting equation is iterated until convergence. This code was used within the TF-FE scheme. (For a summary of the different schemes, please refer to Table I.) On the other hand, to use the TF-ME and the TF-SK functionals we need to solve the k -resolved equation. This is a difficult numerical task mainly because (i)

we need to describe the energy bands over a large energy window and, at the same time, (ii) we require a very good resolution in a small energy window around the Fermi energy. Requirement (i) comes from the large energy scales involved in the Thomas-Fermi screened Coulomb potential (typically of the order of the Fermi energy). This is not an artifact of the static nature of the Thomas-Fermi screening. In fact, even a more realistic dynamically screened potential would need a very large energy range. This point will be further discussed in the following section. To illustrate requirement (ii) we plot, in Fig. 1, the kernel of Eq. (23),

$$W(\xi, \xi', \Omega) = I(\xi, \xi', \Omega) - I(\xi, -\xi', \Omega). \quad (30)$$

The top panel of Fig. 1 depicts the variation of W with energy. This plot was obtained at very low temperature $T = 0.01$ K, by fixing ξ' very close to the Fermi surface $\xi \approx 0$. (We did not use the values $T=0$ and $\xi=0$ to avoid nu-

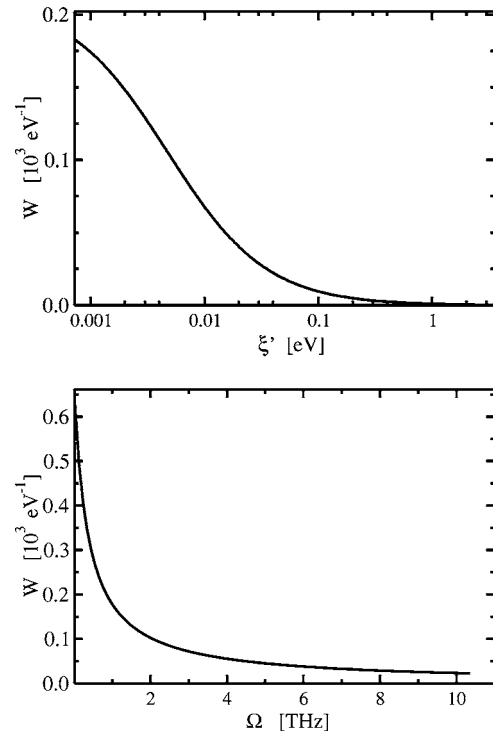


FIG. 1. Universal kernel $W(\xi, \xi', \Omega)$ as a function of ξ' and Ω . Top panel: universal kernel $W(\xi \approx 0, \xi', \Omega = 1 \text{ THz})$ as a function of ξ' . Bottom panel: $W(\xi = \xi' \approx 0, \Omega)$ as a function of Ω . Both panels were obtained for $T = 0.01$ K.

merical problems.) Considering that the kernel decreases to about 20% of its value within roughly 10 meV, it is clear that we need to sample very carefully this energy range. This is particularly important for materials, like niobium and tantalum, where the Fermi energy is at the edge of a peak in the density of states. In the bottom panel we plot the dependence of W on the frequency Ω , for ξ and ξ' very close to the Fermi surface. The kernel W acts as a weight for $\alpha^2F(\Omega)$ [see, e.g., Eq. (23)], and enhances the contribution of the lower-frequency phonons.

In order to satisfy the requirements (i) and (ii) we developed the following numerical framework. Starting from *ab initio* bands calculated over a few hundred \mathbf{k} points in the irreducible wedge of the Brillouin zone (BZ), we compute a good spline fit of $\xi_{n\mathbf{k}}$ over a Fourier series, according to the scheme of Koelling and Wood.²⁴ Using this fit, we then obtain the energies ξ over a very large set of random \mathbf{k} points, distributed according to a Metropolis algorithm. This algorithm was devised to accumulate a large number of \mathbf{k} points in the first few meV's around the Fermi surface. A good convergence can be reached by using about 15 000–20 000 independent points for each band crossing the Fermi surface, while a reasonable description of the remaining bands is obtained with about 1000 independent points per band. The TF-ME scheme is the slowest to converge, as it involves the integration of a function which is peaked around $|\mathbf{k}' - \mathbf{k}| \rightarrow 0$ (the integrand would diverge if we used the bare Coulomb potential instead of the Thomas-Fermi screened interaction).

The function $\Delta_{n\mathbf{k}}$ only needs to be defined in the irreducible wedge of the Brillouin zone. On the other hand, when using the TF-ME scheme, the \mathbf{k}' summation has to be performed over the whole zone. This can be seen from the expression of the Coulomb matrix elements, Eq. (18): By setting $\mathbf{k} \neq 0$ the symmetry of the \mathbf{k}' summation is broken (only the operations of the little group of \mathbf{k} can be retained). This is a well-known situation also in the framework of electronic self-energy calculations. The case of the hybrid functionals is simpler. As these functionals depend on \mathbf{k} and \mathbf{k}' through $\xi_{n\mathbf{k}}$ and $\xi_{n'\mathbf{k}'}$, and as the eigenvalues $\xi_{n\mathbf{k}}$ are totally symmetric with respect to the crystal point group, the summation over \mathbf{k}' can be limited to the irreducible wedge of the Brillouin zone. This formalism can be easily generalized to the case of non-*s*-wave pairing, by imposing that the gap transforms according to a given irreducible representation of the crystal point group.

As an initial guess for the gap function $\Delta_{n\mathbf{k}}$ we use a step function. By using a Broyden scheme²⁵ to mix $\Delta_{n\mathbf{k}}$, we obtain convergence in a mere 10–15 self-consistent iterations. The converged result at a given temperature can be used as a starting point for the next temperature. Clearly, this procedure reduces the total number of iterations required.

The matrix elements of the screened Coulomb potential are obtained with the full-potential linearized augmented plane-wave method, as explained in Ref. 23. They are calculated for all bands within 15–30 eV from the Fermi surface (typically 14 valence and conduction bands). It is unfeasible to obtain the matrix elements for the whole set of random \mathbf{k} points used in the solution of the gap equation. Thus, we calculate the matrix elements for a set of \mathbf{k} and \mathbf{k}' belonging

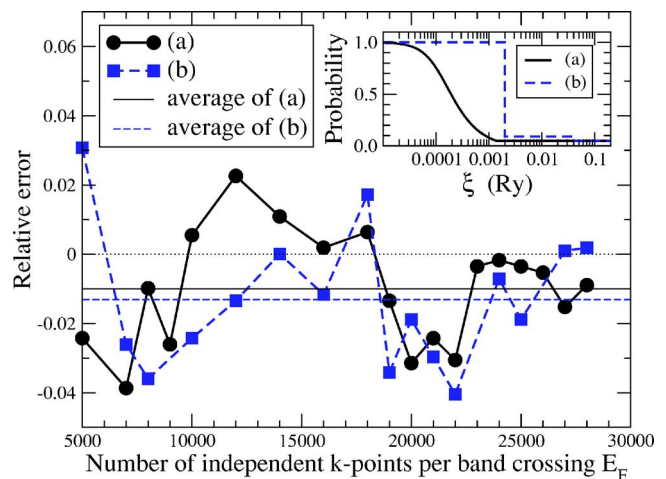


FIG. 2. (Color online) Relative difference between the \mathbf{k} -resolved and the energy-integrated results for Nb, as a function of the number of independent \mathbf{k} points used for each band crossing E_F . The circles and squares are obtained, respectively, with probability distributions equal to $\max\{\chi(\xi, T=0), 0.05\}$ and to a stepwise function having widths of 2 and 40 mRy, as shown in the inset. Thin lines represent the arithmetic averages of the \mathbf{k} -resolved data.

to a regular mesh. The values at the random points \mathbf{k} and \mathbf{k}' are then obtained by mapping \mathbf{k} and \mathbf{k}' to the corresponding hypercube of the regular mesh. Test calculations have shown that already a $6 \times 6 \times 6$ mesh gives acceptably small residual errors (1–2 % of the gap at E_F). A finer mesh is however needed to quantitatively estimate the spread of the gap for each given energy, which is material dependent and mostly due to the physical \mathbf{k} and \mathbf{k}' dependence of the matrix elements.

In Fig. 2 we show a detailed analysis of the convergence of our method for Nb, using the TF-SK approach. In this figure we plot the relative differences between the \mathbf{k} -resolved approach and the results of the energy-only scheme, which can be considered to be numerically convergent (because of its use of a logarithmic energy mesh), but itself depending on the fine details of the input density of states. This is particularly true in the case of Nb, where E_F sits in a rapidly varying part of the density of states (DOS). The results are shown as a function of the number of independent \mathbf{k} points used for each band crossing the Fermi level, and circles and squares represent the results obtained using two different distribution functions used to sample the Brillouin zone (as detailed in the figure caption). We can see the capability of our procedure to converge toward the (computationally completely independent) energy-only result, with a very small numerical error. The two rather different samplings lead to almost identical averages, with a correct, Gaussian-like, distribution of results around the average. We notice that bands away from E_F are sampled uniformly in \mathbf{k} space, as it should since at these energies only the Coulomb term remains, with a weak energy dependence.

For simplicity, we used in all our calculations the averaged or hybrid phononic functionals. In this case, the electron-phonon interaction enters the calculation through the Eliashberg function $\alpha^2F(\Omega)$. This corresponds to neglect-

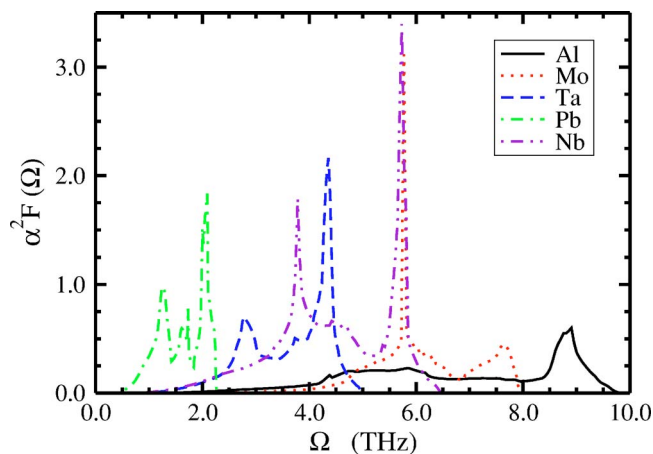


FIG. 3. (Color online) The Eliashberg function $\alpha^2 F(\Omega)$ for the simple metals used in our calculations. The curves are taken from Ref. 31.

ing the anisotropy of the electron-phonon coupling, which should be a good approximation for the particular systems studied in the following.

We quantify the precision of our results to be around 5%. This value includes the uncertainty associated with the Metropolis procedure. We emphasize that this is a nontrivial numerical achievement, as superconducting properties depend exponentially on the electron-phonon coupling and on the Coulomb interaction. Particularly difficult is to obtain numerically stable results for the small gap materials, where superconductivity stems from an almost complete cancellation of large and opposite terms.

V. RESULTS AND DISCUSSION

In the following we will present results obtained for the simple metals Al, Mo, Ta, Nb, and Pb. Note that this group of materials includes both weak-coupling (Al, Mo, and Ta) and strong-coupling (Nb and Pb) superconductors. We solved the gap equation within three different approaches, that we label TF-FE, TF-SK, and TF-ME (see Table I).

In Fig. 3 we show the Eliashberg functions used in our calculations. All these curves were obtained by Savrasov³¹ using linear response theory. The five materials cover a broad frequency range, from 1 to 10 THz. The $\alpha^2 F(\Omega)$ function for Pb is located at much lower frequencies than for the other materials, due to the heavy nuclear mass of Pb. For this reason, Pb has the largest total electron-phonon coupling constant λ of the materials studied [$\lambda = 2 \int d\Omega \alpha^2 F(\Omega) / \Omega$]. Nevertheless, Nb becomes superconducting at higher temperatures than Pb. This can be easily understood on the basis of McMillan's formula:³² Besides the well-known exponential dependence on the electron-phonon coupling constant, the transition temperature increases linearly with the average phonon frequency. Lowering the phonon frequencies has therefore both a positive and a negative effect on T_c . An accurate description of the superconducting state must take into account both these effects.

Before examining our results, we depict in Fig. 4 the be-

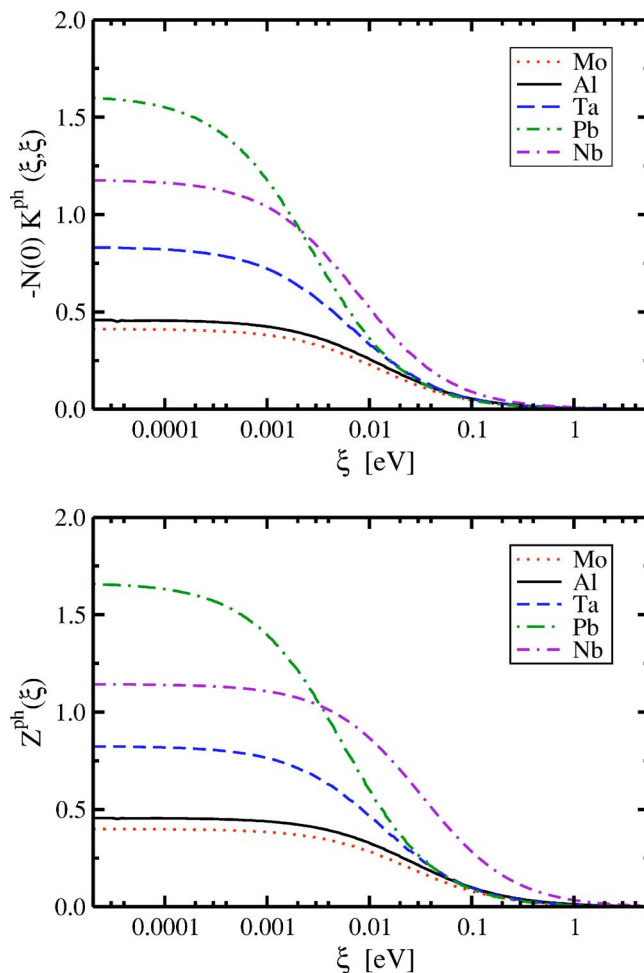


FIG. 4. (Color online) Diagonal of $-N(0)\mathcal{K}^{\text{ph}}(\xi, \xi')$ (top panel) and $\mathcal{Z}^{\text{ph}}(\xi)$ (bottom panel) at $T=0.01$ K for the simple metals studied.

havior of the phononic functionals $-N(0)\mathcal{K}^{\text{ph}}(\xi, \xi')$ and $\mathcal{Z}^{\text{ph}}(\xi)$. Both terms turn out to be very peaked at the Fermi energy, and are nonzero only in a small region around it (of the order of the Debye energy). Furthermore, the values of the functionals at the Fermi energy read $N(0)\mathcal{K}^{\text{ph}}(0, 0) = -\lambda$, and $\mathcal{Z}^{\text{ph}}(0) = \lambda$. The \mathcal{K}^{ph} term is negative, reflecting the electron-phonon attraction responsible for the superconducting state. On the other hand, the term \mathcal{Z}^{ph} is positive and tends to decrease the superconducting gap and therefore T_c .

In Fig. 5 we show the superconducting gap Δ calculated using different approaches for Pb and Nb. For Pb we also show curves calculated at different temperatures. It is important to note that for $T > T_c$ the self-consistent calculation correctly converges to zero even if the starting gap function is different from zero. The curves labeled TF-ME show the detailed sampling of the whole energy range given by our k -point mesh, down to a few μeV . Within the TF-ME approach, the spread in the values of the gap function of Pb at energies near E_F is quite small (around 2%), which can be understood as a consequence of a rather isotropic Fermi surface. This spread is larger for the higher-energy states because of the larger spread of orbital character in the electronic states. The gap function for both materials exhibits a

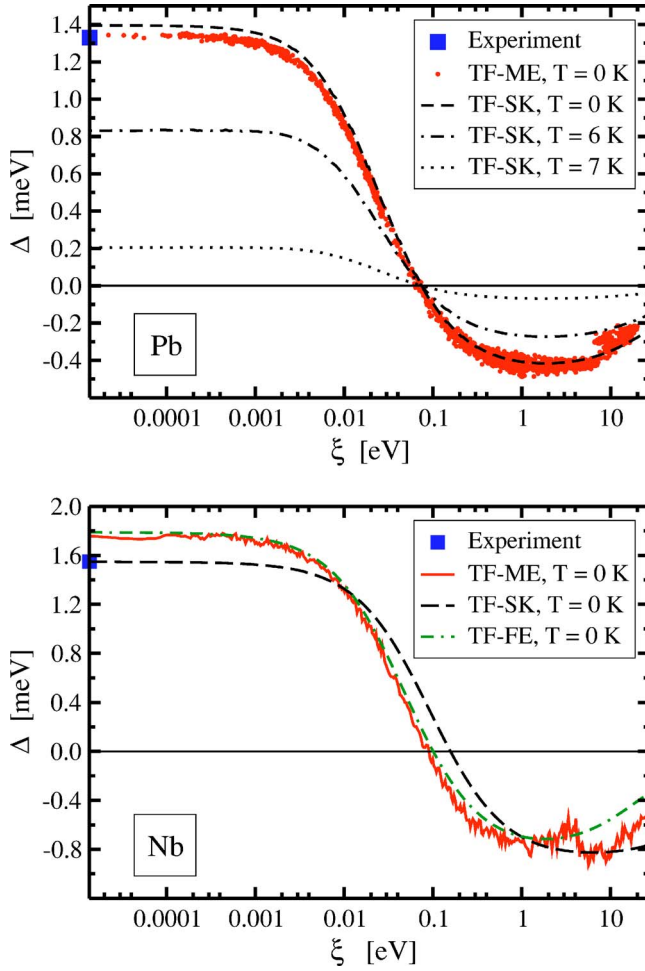


FIG. 5. (Color online) The function $\Delta(\xi_{nk}, T)$ for lead (top panel) and niobium (bottom panel).

very similar shape, with a node at about 0.4 meV, and a negative tail extending to high energy. This shape is basically independent of the temperature, and is a general feature found in all our calculations. Due to the presence of Coulomb repulsion, this shape is a necessary condition to obtain a superconducting solution. It is well known that the structure of the gap equation is such that the repulsive Coulomb interaction between two Cooper pairs (at $\{\mathbf{k}\uparrow, -\mathbf{k}\downarrow\}$ and $\{\mathbf{k}'\uparrow, -\mathbf{k}'\downarrow\}$) gives a constructive contribution to the gap if the values of Δ_{nk} and $\Delta_{n'k'}$ have opposite signs. This condition is realized when, e.g., ξ_{nk} is small and $\xi_{n'k'}$ is large. Similar arguments are the basis of the classical calculations of Ref. 33, and result in the definition of the renormalized Coulomb parameter μ^* .

The three different schemes (TF-FE, TF-SK, and TF-ME) agree well among themselves for Pb, while for Nb the TF-SK curve differs by 10% from the TF-SK and TF-ME results. This difference can be explained by looking at the band structure of the materials. In Pb, the valence and conduction bands are basically due to s and p orbitals, for which the averaged and hybrid schemes work quite well. The same result is found for Al, with an even larger similarity between TF-FE, TF-SK, and TF-ME results. All this is easily understood from the fact that the three schemes TF-FE, TF-SK,

and TF-ME become identical in the limit of the uniform gas. Hence one would expect them to yield similar results for the delocalized s - p orbitals. On the other hand, the bands of Nb exhibit a strong d character, which leads to the difference between the methods. A similar behavior is found for Ta. This trend is also confirmed by the value of the gap function for the low-lying semicore d states of Pb (not shown in the figure) which is very different in the TF-SK, and TF-ME calculations (it is much smaller for TF-ME). This is a clear consequence of the localized nature of these states, implying a very large repulsive self-term for those bands. In principle, the TF-ME approach should be the most precise.

Note that our approximate functionals use the Thomas-Fermi model for screening. We have compared the matrix elements of the Thomas-Fermi-screened potential with those coming from a complete (static) random-phase approximation and found very close agreement between the two approaches. It is very important in this context to define the Thomas-Fermi wave vector k_{TF} in terms of the density of states at the Fermi level, $N(0)$. As the latter is obtained from a full-scale Kohn-Sham calculation, k_{TF} is treated here implicitly as a rather complicated density functional.

Furthermore, we neglect the off-diagonal elements of the dielectric matrix. This is not necessarily a good approximation for transition metal compounds. However, it was shown in the literature^{26,27} that the changes produced by these local field effects are largely canceled by the additional inclusion of exchange-correlation effects (generated by the exchange-correlation kernel²⁸ of time-dependent density functional theory²⁹). We believe that our good results, obtained by neglecting both local field and exchange-correlation effects, can at least partly be explained by this cancellation. Further help comes from the fact that superconductivity describes correlations on the scale of the coherence length, which is usually much larger than the dimensions of the unit cell. On this scale, local field effects are certainly less important.

The gap function at the Fermi energy is depicted in Fig. 6 as a function of temperature for Pb and Nb. The curves show

TABLE II. The critical temperature (upper panel) and the superconducting gap at Fermi level and $T=0.01$ K (lower panel), compared with experiment (Ref. 30). We show also the total electron-phonon coupling constant λ (Ref. 31).

	T_c (K)			Expt.	λ
	TF-ME	TF-SK	TF-FE		
Mo		0.33	0.54	0.92	0.42
Al	0.90	0.90	1.0	1.18	0.44
Ta	3.7	2.7	4.8	4.48	0.84
Pb	6.9	7.2	6.8	7.2	1.62
Nb	9.5	8.4	9.4	9.3	1.18
		Δ_0 (meV)			
Mo		0.049	0.099		0.42
Al	0.14	0.15	0.15	0.179	0.44
Ta	0.63	0.53	0.76	0.694	0.84
Pb	1.34	1.40	1.31	1.33	1.62
Nb	1.74	1.54	1.79	1.55	1.18

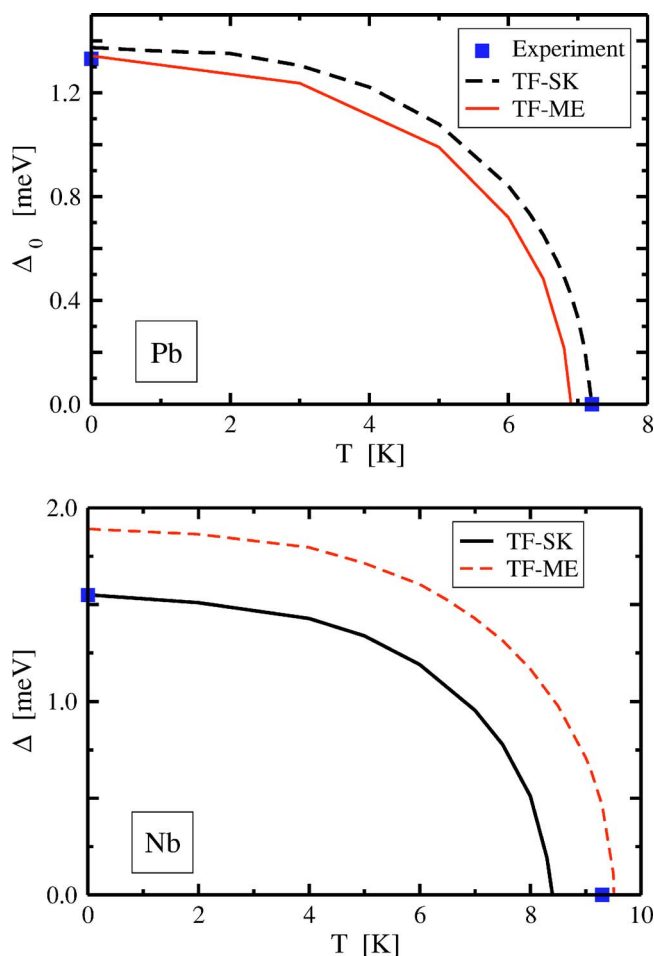


FIG. 6. (Color online) The gap function at the Fermi surface Δ_0 for Pb and Nb as a function of temperature.

a BCS-like square root behavior close to T_c , which we would expect for these simple superconductors. For Pb, both T_c and Δ_0 agree quite well among themselves and with the experimental results. For Nb, on the other hand, the TF-SK gap is roughly 15% smaller than the TF-ME curve. Curiously, the TF-SK gap at zero temperature is very close to the experimental value, while the TF-ME yields a much better transition temperature. The difference between the methods can be once more explained by the d character of the bands in Nb close to the Fermi energy.

Our results for the superconducting transition temperatures and gap functions are summarized in Table II and in Fig. 7 for all materials studied. In the same table we also show the experimental results, and the values of the electron-phonon coupling constant λ . Mo is a weak-coupling superconductor with a very small gap and very low transition temperature. In this case, the different theoretical approaches lead to quite different results, and the overall agreement with experiment is not very good. Surprisingly, it is the TF-FE approach which gives the better results. However, many tests showed that the Mo results are very sensitive to the details of the density of states underlying our calculations. This is quite normal for a material with such a small gap resulting from a very fine balance between large terms. In Al the electronic states have a strong free-electron character and the density of

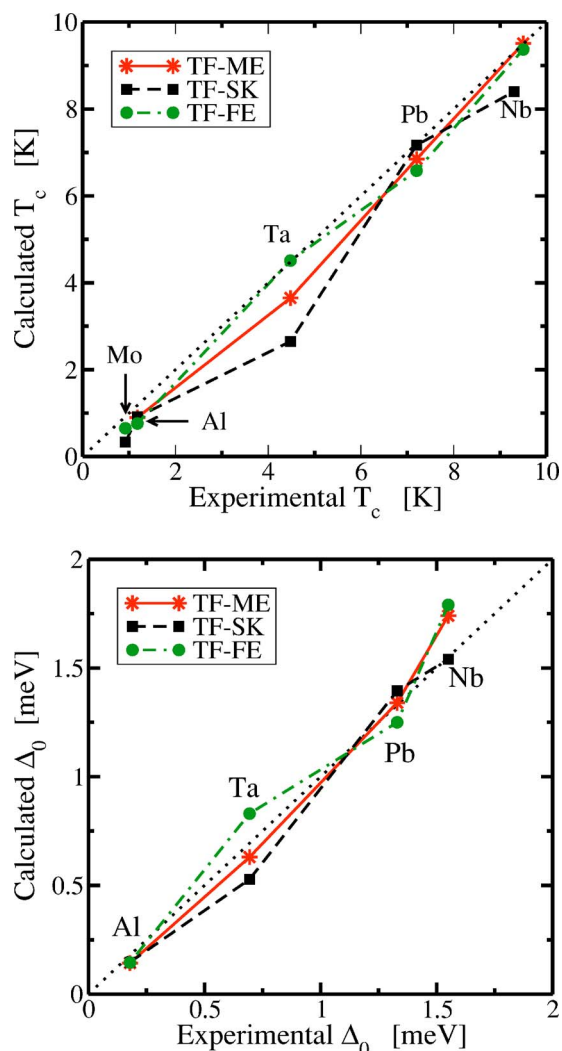


FIG. 7. (Color online) The critical temperature and superconducting gap at Fermi level and $T=0.01$ K, compared with experiment. The numerical values can be found in Table II.

states follows closely the free-electron DOS. It is not surprising, therefore, that all three methods yield very similar results. These results are also in satisfactory agreement with experiment. Ta shows a behavior similar to Nb, but the agreement with experiment is poorer. Moreover, the larger spread of values for Ta relative to Nb can be explained by the smaller values of Δ and T_c . As in the case of Mo, the TF-FE approach yields the best results. This surprising result can be understood to some extent: The TF-FE approach is fully consistent, in the sense that all the quantities entering the method are averaged in similar ways; in the TF-SK approach, on the other hand, certain quantities (but not all) are calculated at the average density. We emphasize, however, that the agreement of our results with experiment, without making use of any adjustable parameters, is unprecedented in the field. We note in passing that for Cu we could not find a nontrivial solution of the gap equation at any temperature, which also is in agreement with the experimentally observed absence of superconductivity in Cu.

It is instructive to visualize how the different terms entering the gap equation combine to yield the values listed in

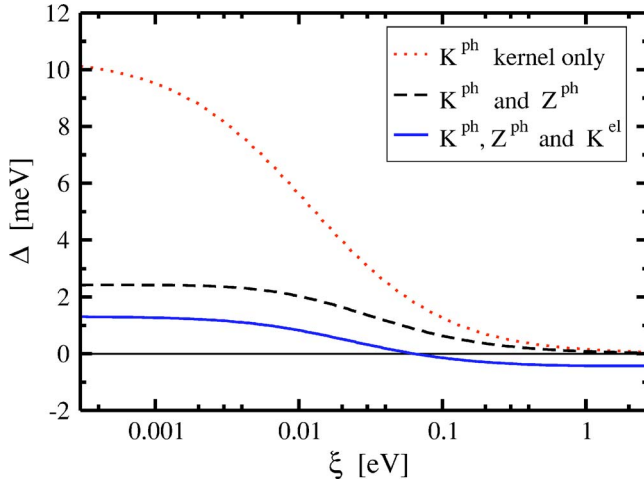


FIG. 8. (Color online) Gap function versus energy at $T = 0.01$ K for Pb, including the different contributions to the gap equation.

Table II: The phononic term \mathcal{K}^{ph} is negative, and is responsible for the superconducting state in the simple metals we studied; \mathcal{Z}^{ph} gives a repulsive contribution, whose relative importance increases for the strong-coupling materials; finally, the electronic Coulomb repulsion leads to a large cancellation between constructive and destructive interference effects. To better understand these effects we plot, in Fig. 8, the gap function at zero temperature of Pb obtained through the solution of the gap equation (20) including only \mathcal{K}^{ph} , the two phononic contributions, or all three phononic and Coulomb contributions. Clearly, the value of the gap is the result of a subtle interplay of opposite contributions, each one considerably larger than the gap itself.

Another interesting point regards the convergence of the gap function with the energy cutoff. This convergence can be observed in Fig. 9, where we plot the gap for Pb and Al calculated within the TF-FE approach. The different materials behave differently, with a faster convergence for the material with stronger electron-phonon coupling. However, even for Pb, an energy cutoff of at least 10 eV was necessary to achieve convergence. It is a key feature of our approach that the matrix elements of the screened Coulomb interaction are used in the kernel of the gap equation up to very high energies. It is this feature that allows for the description of nontrivial, material-specific effects. Traditionally, the use of this large energy window is avoided by rescaling the Fermi-surface average μ of these matrix elements. This rescaling leads to the Morel-Anderson pseudopotential μ^* . While μ^* is an ingenious concept to capture the essential physics of the Coulomb repulsion in simple superconductors, it is not sufficient to treat more complex materials such as, e.g., MgB_2 . The detailed analysis carried out in Ref. 5 shows how the actual value of matrix elements of the screened Coulomb interaction, computed with respect to Bloch states of different orbital character (σ and π), leads to nontrivial effects, determined by the specific character of the orbitals. This indicates that, contrary to common wisdom, superconducting properties are not exclusively determined by a small region around the Fermi level. Only the contributions from states

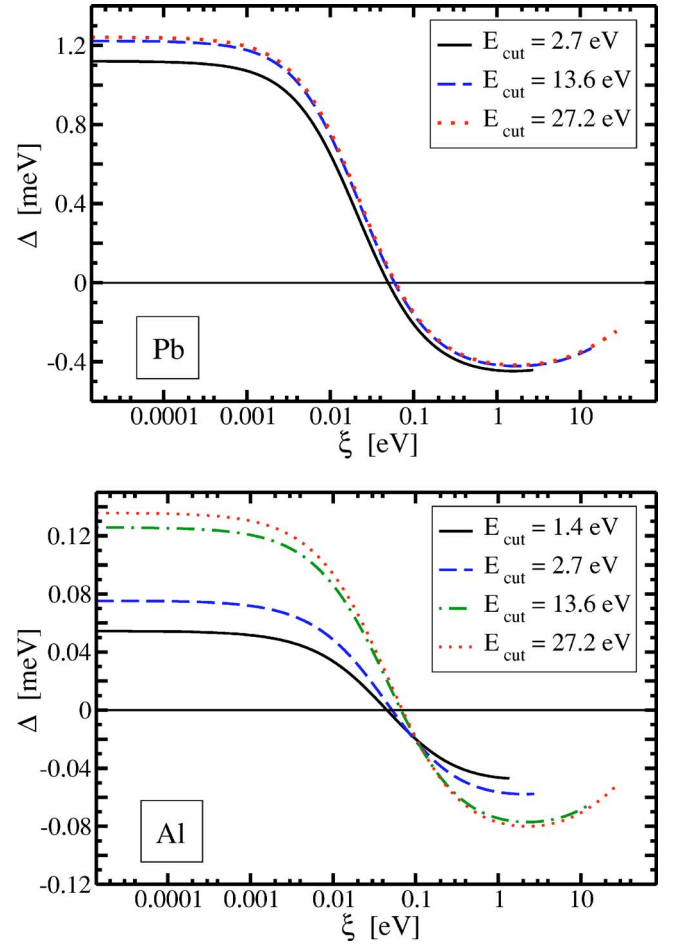


FIG. 9. (Color online) Convergence of the calculated $T = 0.01$ K gap as a function of the energy cutoff, for Pb and Al.

higher than 20–30 eV are essentially negligible, due to the asymptotic decay of the Coulomb term (26).

After solving the gap equation, it is straightforward to calculate thermodynamic functions, such as the electronic entropy of the Kohn-Sham system,

$$S_s = -2k_B \sum_{nk} \{f_\beta(E_{nk}) \ln[f_\beta(E_{nk})] + [1 - f_\beta(E_{nk})] \ln[1 - f_\beta(E_{nk})]\}, \quad (31)$$

where k_B is the Boltzmann constant. In Fig. 10 we depict the difference of entropy between the superconducting and the normal states $\Delta S = S_S - S_N$ for Pb and Nb. This quantity has the expected temperature dependence, going smoothly to zero at T_c . This indicates the stability of our calculations even close to the transition temperature where the gap becomes very small. In the same figure we also depict the normalized specific heat $C_e^{\text{SN,N}}(T)/C_e^{\text{N}}(T_c)$. The specific heat is obtained by evaluating numerically the temperature derivative of the entropy. Despite the numerical uncertainty associated to the calculation of the derivative, the curves of the specific heat are quite stable. The discontinuities of the specific heat at T_c obtained within the TF-ME approach are shown in Table III. Our results are in quite good agreement

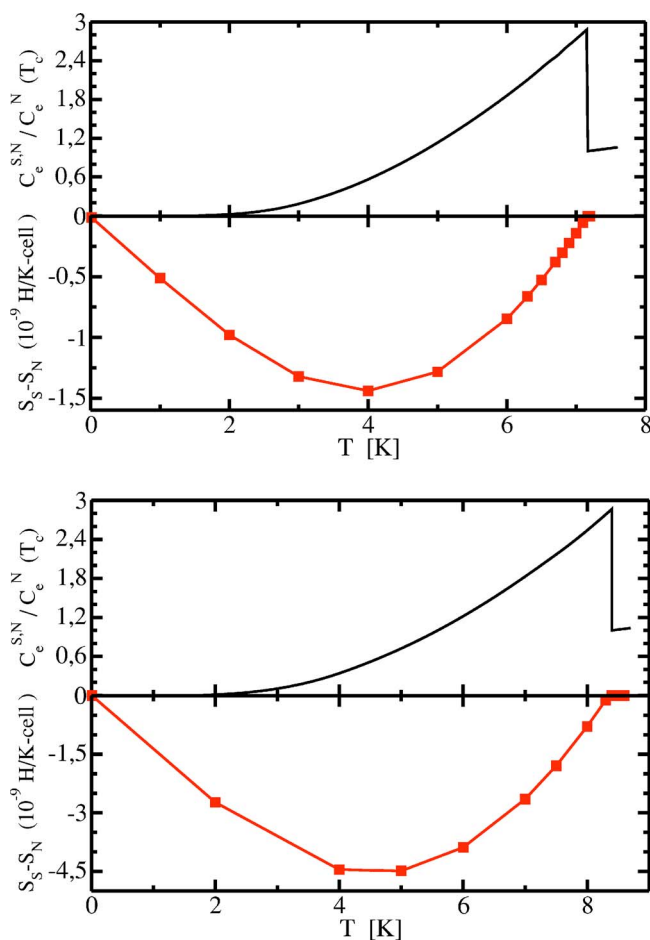


FIG. 10. (Color online) Thermodynamic functions for Pb (top panels) and Nb (bottom panels). Upper panels: ratio between the electronic specific heat ratio in the normal (N) or superconducting (S) states and the specific heat at T_c [$C_e^{S,N}(T)/C_e^N(T_c)$]. Lower panels: difference of entropy between the superconducting and the normal states $\Delta S = S_S - S_N$.

with experiment: While for Al and Ta we confirm the BCS value found in experiments, we reproduce the strong-coupling value of Nb. For Pb the agreement with experiment is worse, but still within acceptable margins.

It is clear that any theory that aims at describing the superconducting state has to include retardation effects. While the main equation of our density functional formalism, the gap equation (5), has the form of a static equation, retardation enters through the electron-phonon part of the exchange-correlation potential. To further demonstrate that our theory takes retardation effects properly into account, we calculated

TABLE III. Normalized electronic specific heat $C_e^S(T_c)/C_e^N(T_c)$, as computed from the TF-ME approach.

	Theory	Experiment
Pb	2.93	3.57–3.71
Nb	2.87	2.8–3.07
Ta	2.64	2.63
Al	2.46	2.43

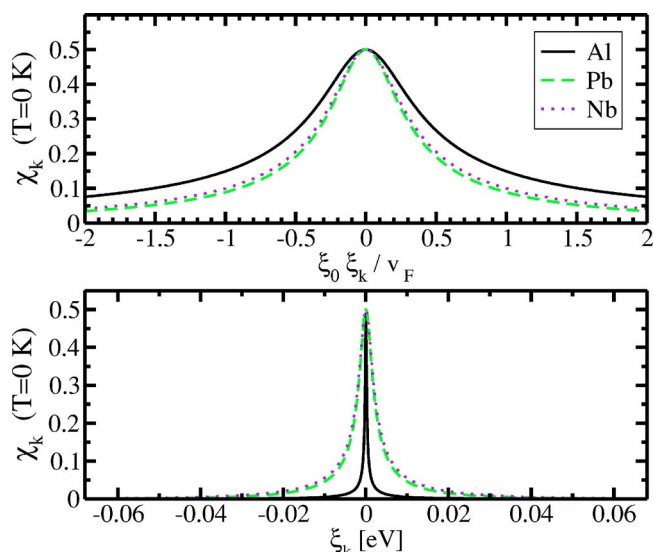


FIG. 11. (Color online) Order parameter for Al, Pb, and Nb represented on the basis of Bloch orbitals as a function of momentum (upper panel) and energy (lower panel). The momentum was rescaled with the experimental coherence lengths $\xi_0 = 1600, 90,$ and 40 nm for Al, Pb, and Nb, respectively.

the isotope effect coefficient α . In fact, if retardation effects were not included, α would be equal to the BCS value $\alpha = 0.5$. For a monatomic solid, the Eliashberg function $\alpha^2 F(\Omega)$ for materials with different isotopic masses can be obtained by rescaling the phonon frequencies with the square root of the nuclear mass M . Note that only the frequencies are rescaled, while the total electron-phonon coupling constant λ remains unchanged. Within the TF-FE approach, we computed the isotope effect of the gap function. We obtained the values 0.37 and 0.47 for Mo and Pb, respectively, which can be compared to the corresponding experimental values $\alpha = 0.33$ and 0.47. This agreement with experiment, in the presence of a significant deviation from the BCS value, proves, in our opinion, that retardation effects are properly taken into account in our calculations.

To conclude the presentation of our results we show, in Fig. 11 the order parameter represented on the basis of Bloch orbitals. The lower panel of the figure depicts the order parameter for Al, Pb, and Nb as a function of the energy of the corresponding Bloch state. As expected, χ_{nk} is very localized in a small energy window around the Fermi level. The spread of the order parameter in k space is related to the inverse of the coherence length of the superconductor. This can be visualized by rescaling the relative energy ξ by $\xi_0/\hbar v_F$, where ξ_0 is the experimental coherence length of the material and $\hbar v_F = \nabla_k \xi_{nk}$ is the Fermi velocity. The resulting curves depict the spread in k space of the wave packets describing the Cooper pairs in units of the experimental coherence length. As expected, the curves for Al, Pb, and Nb are quite similar to each other, and have a width comparable to unity. We can therefore conclude that not only the maximum gap value but also its overall energy dependence are described accurately in our approach.

VI. CONCLUSIONS

In this work we present the first full-scale application of the *ab initio* theory for superconductivity, which was developed in the preceding paper (I). Superconducting properties of simple conventional superconductors are computed without any experimental input. In this way, we were able to test the theory developed in I and to assess the quality of the functionals proposed. It turns out that the different proposed functionals lead to results which are in good agreement with each other for the simple metals studied. The agreement is better when the normal-state Bloch functions are not too strongly localized (like, e.g., the *sp* orbitals in metals in contrast to the more localized *d* states of the transition elements). The most important result is that the calculated transition temperatures and superconducting gaps are also in good agreement with experimental values. The largest deviations from the experimental results are found for the elements in the weak-coupling limit with Mo being the most pronounced example. We emphasize, however, that the agreement of our results with experiment, without making use of any adjustable parameter, is unprecedented in the field. Furthermore, we also obtained other quantities such as the entropy and the specific heat. Our approach reproduces the correct values for

the discontinuity of the specific heat at T_c even in the strong-coupling regime. Finally, we calculated the isotope effect for Mo and Pb, achieving again rather good agreement with experiment. These results clearly show that retardation effects are correctly described by the theory. Our calculations demonstrate that, as far as conventional superconductivity is concerned, the *ab initio* prediction of superconducting properties is feasible.

ACKNOWLEDGMENTS

S.M. would like to thank A. Baldereschi, G. Cappellini, and G. Satta for useful discussions. This work was partially supported by the INFM through the Advanced Research Project (PRA) UMBRA, by a supercomputing grant at Cineca (Bologna, Italy) through the Istituto Nazionale di Fisica della Materia (INFM), and by the Italian Ministry of Education, through a PRIN project. Financial support by the Deutsche Forschungsgemeinschaft, by the EXC!TiNG Research and Training Network of the European Union, and by the NANOQUANTA Network of Excellence is gratefully acknowledged. Part of the calculations were performed at the Hochleistungsrechner Nord (HLRN).

*Also at LAMIA-INFM, Genova, Italy.

¹J. Nagamatsu, N. Nakagawa, T. Muranaka, Y. Zenitani, and J. Akimitsu, *Nature (London)* **410**, 63 (2001).

²J. G. Bednorz and K. A. Müller, *Z. Phys. B: Condens. Matter* **64**, 189 (1986).

³O. Gunnarsson, *Rev. Mod. Phys.* **69**, 575 (1997).

⁴J. M. An and W. E. Pickett, *Phys. Rev. Lett.* **86**, 4366 (2001); K.-P. Bohnen, R. Heid, and B. Renker, *ibid.* **86**, 5771 (2001); A. Y. Liu, I. I. Mazin, and J. Kortus, *ibid.* **87**, 087005 (2001); Y. Kong, O. V. Dolgov, O. Jepsen, and O. K. Andersen, *Phys. Rev. B* **64**, 020501(R) (2001); H. J. Choi, D. Roundy, H. Sun, M. L. Cohen, and S. G. Louie, *Nature (London)* **418**, 758 (2002); and references therein.

⁵A. Floris, G. Profeta, N. N. Lathiotakis, M. Lüders, M. A. L. Marques, C. Franchini, E. K. U. Gross, A. Continenza, and S. Massidda, *Phys. Rev. Lett.* **94**, 037004 (2005).

⁶J. Bardeen, L. N. Cooper, and J. R. Schrieffer, *Phys. Rev.* **108**, 1175 (1957).

⁷M. Lüders, M. A. L. Marques, N. N. Lathiotakis, A. Floris, G. Profeta, L. Fast, A. Continenza, S. Massidda, and E. K. U. Gross, preceding paper, *Phys. Rev. B* **72**, 024545 (2005).

⁸P. Hohenberg and W. Kohn, *Phys. Rev.* **136**, B864 (1964).

⁹W. Kohn and L. J. Sham, *Phys. Rev.* **140**, A1133 (1965).

¹⁰R. M. Dreizler and E. K. U. Gross, *Density Functional Theory* (Springer-Verlag, Berlin, 1990); J. P. Perdew and S. Kurth, in *A Primer in Density Functional Theory*, edited by C. Fiolhais, F. Nogueira, and M. A. L. Marques, Lecture Notes in Physics Vol. 620 (Springer, Berlin, 2003), p. 144.

¹¹A. Görling and M. Levy, *Phys. Rev. A* **50**, 196 (1994).

¹²T. Kreibich and E. K. U. Gross, *Phys. Rev. Lett.* **86**, 2984 (2001).

¹³N. D. Mermin, *Phys. Rev.* **137**, A1441 (1965).

¹⁴C. Thomsen, M. Cardona, B. Friedl, I. I. Mazin, O. Jepsen, O. K.

Andersen, and M. Methfessel, *Solid State Commun.* **75**, 219 (1990); E. Altendorf, X. K. Chen, J. C. Irwin, R. Liang, and W. N. Hardy, *Phys. Rev. B* **47**, 8140 (1993); X. J. Zhou, M. Cardona, D. Colson, and V. Viallet, *ibid.* **55**, 12770 (1997).

¹⁵S. Baroni, S. de Gironcoli, A. Dal Corso, and P. Giannozzi, *Rev. Mod. Phys.* **73**, 515 (2001).

¹⁶M. B. Suvasini and B. L. Gyorffy, *Physica C* **195**, 109 (1992); M. B. Suvasini, W. M. Temmerman, and B. L. Gyorffy, *Phys. Rev. B* **48**, 1202 (1993); B. L. Györffy, Z. Szotek, W. M. Temmerman, O. K. Andersen, and O. Jepsen, *ibid.* **58**, 1025 (1998); W. M. Temmerman, Z. Szotek, B. L. Gyorffy, O. K. Andersen, and O. Jepsen, *Phys. Rev. Lett.* **76**, 307 (1996).

¹⁷E. K. U. Gross and S. Kurth, *Int. J. Quantum Chem., Quantum Chem. Symp.* **25**, 289 (1991).

¹⁸S. Kurth, Ph.D. thesis, Bayerische Julius-Maximilians-Universität Würzburg, 1995.

¹⁹G. M. Eliashberg, *Sov. Phys. JETP* **11**, 696 (1960) J. R. Schrieffer, *Theory of Superconductivity* (Addison-Wesley, Reading, MA, 1964); D. J. Scalapino, in *Superconductivity*, edited by R. D. Parks (Marcel Dekker, New York, 1969), Vol. 1; D. J. Scalapino, J. R. Schrieffer, and J. W. Wilkins, *Phys. Rev.* **148**, 263 (1966); J. P. Carbotte, *Rev. Mod. Phys.* **62**, 1027 (1990); P. B. Allen and B. Mitrovic, in *Solid State Physics*, edited by H. Ehrenreich, F. Seitz, and D. Turnbull (Academic, New York, 1982), Vol. 37, p. 1.

²⁰M. Lüders, Ph.D. thesis, Bayerische Julius-Maximilians-Universität Würzburg, 1998.

²¹L. J. Sham and W. Kohn, *Phys. Rev.* **145**, 561 (1966).

²²H. J. F. Jansen and A. J. Freeman, *Phys. Rev. B* **30**, 561 (1984); E. Wimmer, H. Krakauer, M. Weinert, and A. J. Freeman, *ibid.* **24**, 864 (1981).

²³S. Massidda, A. Continenza, M. Posternak, and A. Baldereschi,

- Phys. Rev. B **55**, 13494 (1997).
- ²⁴D. D. Koelling and J. H. Wood, *J. Comput. Phys.* **67**, 253 (1986).
- ²⁵C. G. Broyden, *Math. Comput.* **19**, 577 (1965).
- ²⁶K. H. Lee, K. J. Chang, and M. L. Cohen, *Phys. Rev. B* **52**, 1425 (1995).
- ²⁷K. H. Lee and K. J. Chang, *Phys. Rev. B* **54**, 1419 (1996).
- ²⁸E. K. U. Gross and W. Kohn, *Phys. Rev. Lett.* **55**, 2850 (1985).
- ²⁹E. Runge and E. K. U. Gross, *Phys. Rev. Lett.* **52**, 997 (1984).
- ³⁰N. W. Ashcroft and N. D. Mermin, *Solid State Physics* (Saunders College Publishing, Fort Worth, TX, 1976).
- ³¹S. Y. Savrasov, *Phys. Rev. Lett.* **69**, 2819 (1992); S. Y. Savrasov and D. Y. Savrasov, *Phys. Rev. B* **54**, 16487 (1996).
- ³²W. L. McMillan, *Phys. Rev.* **167**, 331 (1968).
- ³³P. Morel and P. W. Anderson, *Phys. Rev.* **125**, 1263 (1962).